Weak-field dynamo emerging in a rotating spherical shell with stress-free top and no-slip bottom boundaries

Youhei Sasaki*[1],Shin-ichi Takehiro[2],Kiyoshi Kuramoto[3],Yoshi-Yuki Hayashi[4]

*contact: uwabami@gfd-dennou.org

[1]Department of Mathematics, Kyoto University, Japan, [2]Research Institute for Mathematical Sciences, Kyoto University, Japan,[3]Depertment of Cosmosciences, Hokkaido University, Japan, [4]Center for Planetary Scinece, Kobe University, Japan

Abstract

Numerical experiments of MHD dynamo in a rotating spherical shell with stress-free top and no-slip bottom boundaries are performed. The Ekman number, the Prandtl number, and the ratio of inner and outer radii are fixed to 10^{-3}, 1, 0.35, respectively. The magnetic Prandtl number is varied from 5 to 50, and the modified Rayleigh number is increased from 1.5 to 10 times critical. All the obtained successful solutions are weak filed-dynamo solutions, that is, the total magnetic energy is far less that the total kinetic energy. These dynamo solutions are characterized by the two-layer spatial structure. The upper layer is governed by prograde strong zonal flows and less-organized prograde propagating spiral convection vortices, while the lower layer is dominated by turbulent retrograde propagating columnar convection vortices. The strong zonal flow in the upper layer prevents the magnetic field generated in the lower layer from penetrating to the surface of the spherical shell.

Introduction

- In recent years, three-dimensional numerical simulations of MHD dynamo in rotating spherical shells have been carried out vigorously in order to investigate generation and maintenance mechanisms of magnetic fields in celestial bodies. However, in most of the simulations performed so far, the mechanical conditions at the top and bottom boundaries are both stress-free [e.g. 1; 2] or both no-slip [e.g. 3; 4]. MHD dynamo problem with stress-free top and no-slip bottom boundaries has not been studied.
- A stress-free condition at both boundaries has been adopted in considering for the solar convection layer. Use of a stress-free condition at both boundaries might also be a theoretical tradition from thermal convection problems in a plane layer. A no-slip condition at both boundaries has been adopted in models of the central fluid cores of the terrestrial planets. However, a stress-free condition at the top and a no-slip condition at the bottom may also be interesting. from geophysical and astrophysical viewpoints:
  - Since there may exist solid cores in the deepest part of the gas giant planets [5], a no-slip condition at the bottom seems to be suitable for the fluid motions in the fluid layers above the cores.
  - In the Earth, existence of a stably stratified layer just below the core-mantle boundary is suggested [6]. This implies that a stress-free condition at the upper boundary might be appropriate for the fluid motion underneath.
  - Recent development of Helio-seismology reveals existence of a strong shear layer (Tachocline) between the upper convective layer and the rigidly rotating lower radiative layer [7]. This suggests that a no-slip condition at the bottom might be appropriate for the fluid motion in the solar convective layer.
- In the present study, numerical experiments are performed in order to investigate an MHD dynamo in a rotating spherical shell with a stress-free condition at the top and a no-slip condition at the bottom. For the sake of comparison, we perform the same calculations but with a no-slip condition at both boundaries.We investigate the effects of the difference of the top mechanical boundary condition on convection structures and of the morphology of a magnetic field.

Model and Methods

- System:
  - Boussinesq MHD fluid in a rotating spherical shell:

$$\nabla\cdot u = 0, \quad \nabla\cdot B = 0, \tag{1}$$

$$\mathrm{E}\left\{\frac{\partial u}{\partial t} + (u\cdot\nabla)u - \nabla^2 u\right\} + 2e_z\times u = -\nabla\pi + \mathrm{Ra}\frac{r}{r_o}T + \frac{1}{\mathrm{Pm}}(\nabla\times B)\times B, \tag{2}$$

$$\frac{\partial B}{\partial t} = \nabla\times(u\times B) + \frac{1}{\mathrm{Pm}}\nabla^2 B, \tag{3}$$

$$\frac{\partial T}{\partial t} + (u\cdot\nabla)T = \frac{1}{\mathrm{Pr}}\nabla^2 T. \tag{4}$$

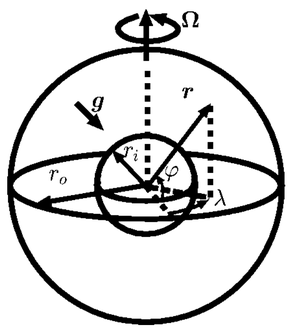

- Parameters:
  - the modified Rayleigh number $\mathrm{Ra} = \alpha g_o \Delta T D/(\Omega\nu)$,
  - the Ekman number $\mathrm{E} = \nu/(2\Omega D^2)$
  - the Prandtl number $\mathrm{Pr} = \nu/\kappa$
  - the magnetic Prandtl number $\mathrm{Pm} = \nu/\eta$
- The boundary conditions:
  - The temperature boundary condition is isothermal
  - The outside the spherical shell and the inner core are electrical insulators
  - The inner dynamical boundary condition is always no-slip.
  - The outer dynamical boundary condition is no-slip (RR case) or stress-free (FR case)
- Numerical methods: traditional spectral transform method[e.g. 8].
  - The temperature and the toroidal/poloidal potentials of u and B are expanded by the spherical harmonic functions horizontally and the Chebychev polynomial radially.
  - The time integration is performed with the Crank-Nicolson scheme for the diffusion terms and with the second order Adams-Bashforth scheme for the other terms.
- Experimental setup:
  - the Ekman number, the Prandtl number, and the ratio of inner and outer radii are fixed to 10^{-3}, 1, 0.35, respectively.
  - The magnetic Prandtl number is varied from 5 to 50, and the modified Rayleigh number is increased from 1.5 to 10 times critical.
  - For each combination of the parameters and the boundary conditions, time integration of non-magnetic thermal convection is carried out until a quasi-steady state is established.
  - Starting from this quasi-steady state with a small dipole magnetic field, MHD dynamo calculation is performed.

List of numerical experiments

- In the following, we report the results obtained for the case in which $\mathrm{Ra} = 250$ ($\mathrm{Ra}/\mathrm{Ra_c} \sim 5$) and $\mathrm{Pm} = 10$, where typical dynamo solutions are obtained for both the RR case and FR case. († symboled in Table. 1)

Table (1) List of the numerical experiments. "FR" in the first column means that stress-free top and no-slip bottom boundary conditions, and "RR" in the first column means that both no-slip boundary conditions. E_k and E_m are the mean kinetic and magnetic energies of the solutions, respectively. "Morp." represents morphology of magnetic field in the self-sustained dynamos. "Decay" means that magnetic field vanished, while "Multi" indicates that multiple (dipole and quadrapole) components dominate the developed magnetic field.

b.c.	Ra	Pm	E_k	E_m	E_m/E_k	Morp.
FR	100	4-15	-	-	-	Decay
FR	150	4-15	-	-	-	Decay
FR	250	5	-	-	-	Decay
FR†	250	10	7.53×10^{2}	4.42×10	0.586×10^{-1}	Multi
FR	250	15	7.32×10^{2}	9.35×10	1.277×10^{-1}	Multi
FR	500	3	-	-	-	Decay
FR	500	5	6.08×10^{3}	2.23×10^{2}	0.367×10^{-1}	Multi
FR	500	10	5.72×10^{3}	5.35×10^{2}	0.935×10^{-1}	Multi
RR	100	5 - 20	-	-	-	Decay
RR	150	5 - 10	-	-	-	Decay
RR	150	15	1.12×10^{2}	4.65×10^{2}	4.15	Dipole
RR	250	5	-	-	-	Decay
RR†	250	10	2.15×10^{2}	1.25×10^{3}	5.81	Dipole
RR	500	5	-	-	-	Decay
RR	500	10	0.85×10^{3}	7.06×10^{3}	4.31	Dipole

Results

- Comparison of temporal development of kinetic & magnetic energy
  - A weak-field dynamo solution is obtained for the FR case. The magnetic energy is one order of magnitude smaller than the kinetic energy.
  - This is in contrast with the results for the RR case, in which a strong-field dynamo solution is established.

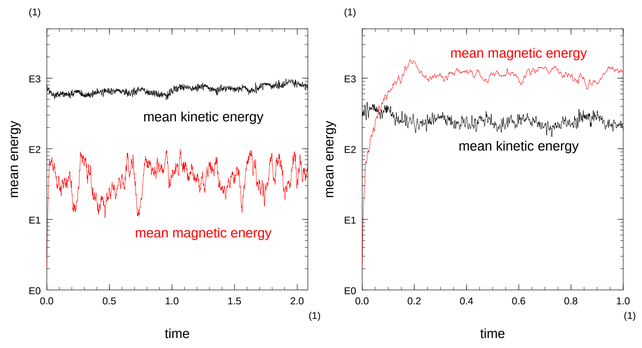

Figure (1) Temporal development of kinetic energy and magnetic energy for the cases of $Ra/Rac \sim 5$ and $Pm = 10$. the left panel shows the stress-free top boundary case (FR). The right panel shows the both no-slip case (RR), while The black and red lines denote kinetic and magnetic energies, respectively. The unit of the horizontal axis is the magnetic diffusion time.

- Snapshots of the spatial structures of the dynamo solutions.
  - In the FR case, the magnetic field at the top boundary is characterized by wedge-shaped patterns around the equator (upper-left panel).
    - These patterns propagate in the prograde direction (as shown Figure.4).
  - Disturbances at high latitudes are highly time dependent and incoherent.
    - Magnetic flux patches observed at high latitudes for the RR case (lower-left panel) are not recognizable.
  - The correlation between the axial components of vorticity and magnetic fields is not clear, which is in contrast with the RR case (center panels).
  - The dipolar component of the magnetic field is not prominent (upper-right panel).
    - Most of the poloidal magnetic field lines are closed inside of the spherical shell and the radial component of the magnetic field is small in contrast with the RR case (lower-right panel).

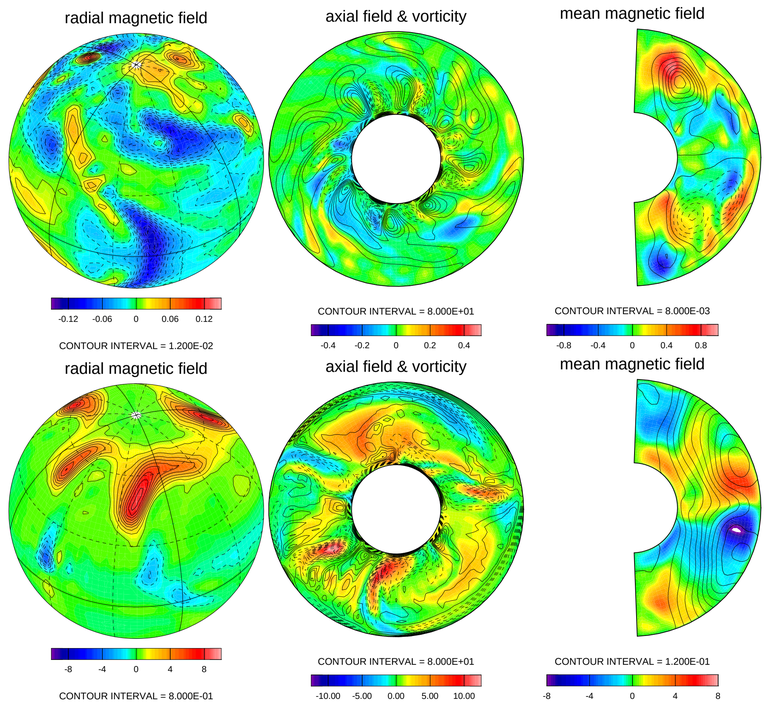

Figure (2) Snapshots of the spatial structures of dynamo solutions for $\mathrm{Ra} = 250$ and $\mathrm{Pm} = 10$. The upper and lower rows are for the FR and RR cases, respectively. The left-hand panels show the radial components of the magnetic fields at the top boundary. The center panels show the axial components of the magnetic fields (tone) and the vorticity fields (contours) in the equatorial cross section. The right-hand panels show the zonal mean toroidal magnetic fields (tone) and the poloidal magnetic field lines.

- Comparison of the spatial structures of convectie motions
  - The dynamo solution obtained in the FR case is characterized by a two-layer spatial structure.
    - Convective vortices associated with intense temperature disturbances are limited within the lower half layer of the shell, and spiral vortices with a larger scale, as compared to the convective vortices, exist in the upper half layer (upper-left and center panels).
    - This is in contrast with the results for the RR case whereby convective vortices with intense temperature disturbances spread over the entire layer (lower-left and center panels).
  - In the FR case, a strong prograde mean zonal flow appears in the upper layer around the equator, whereas in the RR case, a retrograde weak zonal flow dominates outside the tangent cylinder (right panels).

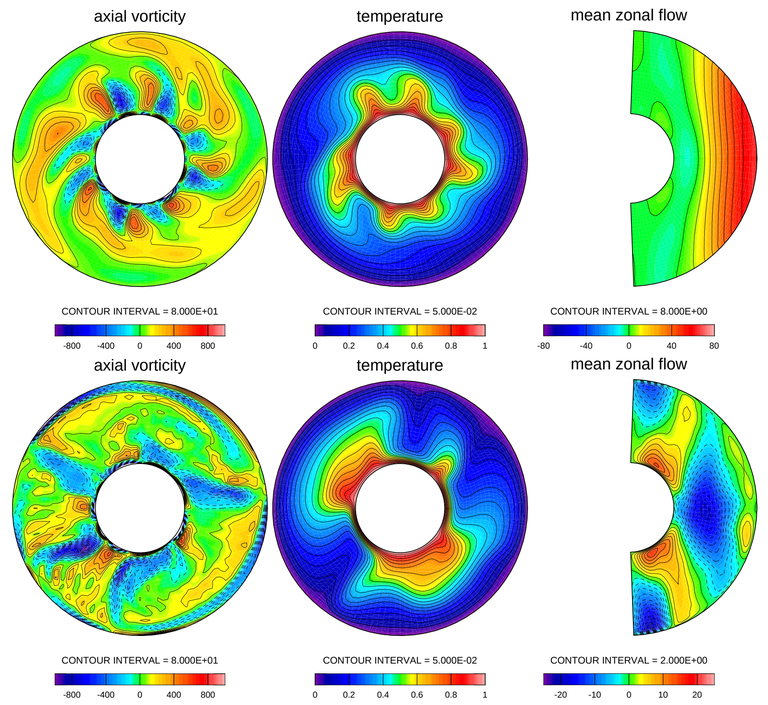

Figure (3) Snapshots of velocity and vorticity fields for $\mathrm{Ra} = 250$ and $\mathrm{Pm} = 10$. The upper and lower rows show the results for the FR and RR cases, respectively. The left-hand and center panels show the axial components of vorticity fields and temperature in the equatorial cross section, respectively. The right-hand panels show zonal mean zonal flows in a meridional cross section.

Discussions

- Temporal variation of the radial component of velocity at the equator.
  - Characteristics of the drift of the convection patterns are different between in the lower layer ($r = r_i + 0.1$) and the upper layer($r = r_o - 0.1$).
  - In the lower layer, the convection pattern propagates in the retrograde direction with the phase speed of 7.8
  - In the upper layer, it propagates in the prograde direction with the phase speed of 40.

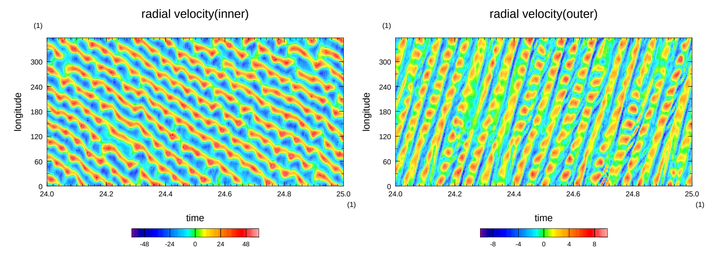

Figure (4) Temporal variations of the radial component of velocity at the equator for case FR. The left and right panels are for the lower layer ($r = r_i + 0.1$) and the upper layer ($r = r_o - 0.1$), respectively

- The temporal average of the fields from the longitudinally-moving frame traveling with the propagating speed of the disturbances in each layer.
  - Anti-cyclonic vortices having a longitudinal wavenumber of 8 are prominent primarily in the lower layer (left-hand panel).
  - Cyclonic vortices having a longitudinal wavenumber of 3 are dominant in the middle and upper layers (right-hand panel).
  - In both layers, the magnetic filed lines are winding around the vortices.

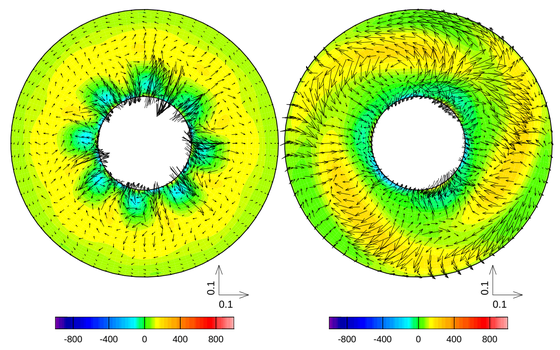

Figure (5) Time mean projection of the magnetic field (vectors) and axial component of the vorticity field (tone) in the equatorial plane for $\mathrm{Ra} = 250$ and $\mathrm{Pm} = 10$ for the FR case. The left- and right-hand panels are averaged on the longitudinally-moving frame traveling at the propagating speeds of the lower and upper disturbances indicated in Figure 4, respectively.

- In order to investigate maintainance mechanism of magnetic field of these weak-field dynamo solutions, we examine budgets of magnetic and kinetic energies by decomposing them into the toroidal and poloidal components.
  - The poloidal magnetic field is mainly generated by retrograde propagating poloidal columnar convection vortices in the lower layer.
  - On the other hand, the toroidal magnetic field is generated by the prograde propagating toroidal cyclonic vortices in the upper layer.

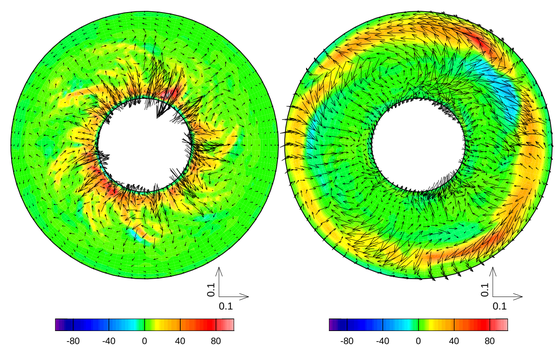

Figure (6) Temporally averaged structuresof the magnetic field and axial vorticity for $\mathrm{Ra} = 250$ and $\mathrm{Pm} = 10$ for the FR case. The center- and right-hand panels are averaged on the longitudinally-moving frame traveling at the propagating speeds of the lower and upper disturbances, respectively.

Summary

- We have performed numerical experiments of MHD dynamo in a rotating spherical shell with stress-free top and no-slip bottom boundaries. The obtained self-sustained dynamo solutions are weak-field solutions that are characterized by a two-layer structure.
  - The upper layer is dominated by a prograde strong mean zonal flow with large scale prograde propagating spiral vortices.
  - The lower layer is filled with small scale retrograde propagating columnar convective vortices.
  - In contrast with the RR case, the magnetic field lines are not concentrated in the vortices, but rather wind around the vortices in each layer.
- This morphology of the magnetic field lines and vortices suggests that the intensification of magnetic field occurs through the winding and stretching of the field lines by the vortices in each layer.

Acknowledgments

- Numerical computations were carried out on a Cray XT4 at the Center for Computational Astrophysics, CfCA, of the National Astronomical Observatory of Japan.
- The library for spectral transform 'ISPACK'[9] and its Fortran90 wrapper library 'SPMODEL library'[10] were used for the numerical calculations.
  - The numerical codes used in the present study is also available from the 'SPMODEL library' web site: http://www.gfd-dennou.org/library/spmodel/
- The products of the Dennou-Ruby project were used to draw the figures: http://www.gfd-dennou.org/library/ruby

References

[1] W. Kuang and J. Bloxham, Nature **389**, 371 (1997).
[2] E. Grote and F. H. Busse, Fluid Dynamics Research **28**, 349 (2001).
[3] G. A. Glatzmaier and P. H. Roberts, Nature **377**, 203 (1995).
[4] A. Kageyama and T. Sato, Physics of Plasmas **2**, 1421 (1995).
[5] T. Guillot, Annual Review of Earth and Planetary Sciences **33**, 493 (2005).
[6] B. A. Buffett and C. T. Seagle, Journal of Geophysical Research (Solid Earth) **115**, 4407 (2010).
[7] R. Howe, J. Christensen-Dalsgaard, F. Hill, R. W. Komm, R. M. Larsen, J. Schou, M. J. Thompson, and J. Toomre, Science **287**, 2456 (2000).
[8] G. Glatzmaier, Journal of Computational Physics **55**, 461 (1984).
[9] K. Ishioka, http://www.gfd-dennou.org/library/ispack/(2009).
[10] S. Takehiro, Y. Sasaki, Y. Morikawa, K. Ishioka, M. Odaka, Y. Takahashi, S. Nishizawa, K. Nakajima, M. Ishiwatari, Y.-Y. Hayashi, and SPMODEL Development Group, http://www.gfddennou.org/library/spmodel(2009).